Selection of Dominant Characteristic Modes

Sandip Ghosal, *Student Member, IEEE*, Arijit De, *Member, IEEE*, Alistair Duffy, *Fellow, IEEE* and Ajay Chakrabarty

***Abstract*—The theory of characteristic modes is a popular physics based deterministic approach which has found several recent applications in the fields of radiator design, electromagnetic interference modelling and radiated emission analysis. The modal theory is based on the approximation of the total induced current in an electromagnetic structure in terms of a weighted sum of multiple characteristic current modes. The resultant outgoing field is also a weighted summation of the characteristic field patterns. Henceforth, a proper modal measure is an essential requirement to identify the modes which play a dominant role for a frequency of interest. The existing literature of significance measures restricts itself for ideal lossless structures only. This paper explores the pros and cons of the existing measures and correspondingly suggests suitable alternatives for both radiating and scattering applications. An example is presented in order to illustrate the proposed modal method for approximating the shielding response of a slotted geometry.**

***Index Terms*—Characteristic mode analysis,modal significance,radiation, scattering, shielding effectiveness.**

I. Introduction

CHARACTERISTIC mode analysis was initially developed through the standard eigen decomposition of the infinite dimensional far-field scattering matrix in [4]. The eigenvectors of the scattering matrix constitute the characteristic field patterns. Later the field continuity relations were used to formulate the method-of-moment (MoM) impedance matrix whose generalized eigen decomposition provides the characteristic current modes and the eigenvalues of the structure in [2] and [3]. The theory of characteristic modes (TCM) was introduced as an alternative to the conventional MoM approach [1] in order to determine the current density vector induced by the incident excitation field. Since the total induced current vector is expressed as the weighted sum of multiple eigencurrent modes, it is necessary to predict the contribution of each mode in the resultant outgoing field.

Initial applications of the characteristic modes were focussed on radiation-based applications such as antenna design. As a consequence, the literature of modal significance measures is mostly confined within the radiation problems as found in [2], [5], and [6]. Apart from the antenna design perspective, the TCM has also been recently applied to determine the optimal placement locations of the grounding, signal and power routing and impedance loading to reduce the radiated emission in digital systems [7]. Similarly in [8] and [9], the characteristic modes were used to quantify the radiated emission. Since the eigenmodes and eigenvalues are independent of the excitation signal, the TCM was used to compare the high intensity radiated field (HIRF) testing and direct current injection (DCI) techniques for an aircraft structure in [10]. As the TCM allows approximating the induced current and radiated field by a relatively less number of variables, it is also finding utilisation in cross-talk analysis of the printed circuit board (PCB) components [11].

For all such modal applications, a specific *modal metric* is followed to determine the significant characteristic modes. Most of the existing modal significance measures are based on only the eigenvalue which is independent of the incident signal. Alternate measures used in [6] and [8] lie on the assumption that the incident field vector is non-zero at only few feed locations on the surface of the radiating structure. For scattering applications like in shielding analysis [12] and [13], the definition of *modal metric* requires broader extension to include the distributed nature of the incident signal. In addition, the existing modal measures are only applicable to the lossless structures. But the lossy structures are also being analysed using the characteristic modes [14]. It has been found in [15] that finite loss affects the nature of the current distribution and various radiation parameters. So the modal significance is to be defined accordingly to fit for the lossy structures too. Keeping this on mind, this work follows a constrained approach to define two different measures for radiating and scattering problems separately. The proposed measures are simultaneously applicable for both the lossy and lossless structures. The limitations of the existing measures have been explored and the proposed measures have been validated through multiple examples.

The paper has been organised as follows. With a brief recap of the reported literature, Section II postulates the problem statements which have been addressed with various examples. Suitable measures have been suggested individually for each case in Section III. Later ,the proposed method has been utilised for predicting the shielding effectiveness (SE) of a slotted structure in Section IV. Section V summarises the total work.

II. Review of the Modal Background

For the sake of generality, the formulation has been developed considering an finitely conducting object lying in free-space with surface area S, incident electric field $\vec{E}_i$ and the corresponding induced surface current density, $\vec{J}$. Considering no internal resonance [16], the continuity of the tangential

Manuscript received Sep. XX, 2018.

S. Ghosal, A. De and A. Chakrabarty are with the Department of Electronics and Electrical Communication Engineering, Indian Institute of Technology Kharagpur, India(e-mail: sgmw@iitkgp.ac.in).

A. Duffy is with the De Montfort University, Leicester LE1 9B, U.K. He is also associated with Harbin Institute of Technology, Harbin, China. (e-mail: apd@dmu.ac.uk).

Color versions of one or more of the figures in this paper are available online at http://ieeexplore.ieee.org.

electric field on the surface S maps $\vec{E}_i$ to $\vec{J}$ as [2] and [17],

$$\hat{n} \times \vec{E}^i = -\hat{n} \times L(\vec{J}) + Z_s \vec{J} \tag{1a}$$

$$L(\vec{J}(r)) = j\omega A(\vec{J}(r)) + \nabla\phi(\vec{J}(r)) \tag{1b}$$

$$A(\vec{J}(r)) = \mu \oint_S \vec{J}(r) G(r,r')\, ds \tag{1c}$$

$$\phi(\vec{J}(r)) = \frac{-1}{j\omega\epsilon} \oint_S \nabla' \vec{J}(r) G(r,r')\, ds \tag{1d}$$

$$G(r,r') = \frac{e^{-jk|r-r'|}}{4\pi|r-r'|} \tag{1e}$$

$$\begin{aligned} Z_s &= \frac{1}{\sigma t}[1 + \frac{jt^2}{6s^2} + O((\frac{t}{s})^4)] \text{ if } \frac{t}{s} << 1 \\ &= \frac{1+j}{2s\sigma}[1 + 2e^{\frac{-(1+j)t}{s}} + O(e^{\frac{-2t}{s}})] \text{ otherwise} \end{aligned} \tag{1f}$$

The magnetic vector potential and the electric scalar potential are represented by A and ϕ respectively. The parameters μ, ω and k denote the free-space permeability, frequency and propagation constant. t, σ, and s indicate the thickness, conductivity and skin-depth of the conductor respectively. The finite surface impedance is approximated in (1f) using [17]. Applying Galerkin's type of MoM technique with N number of basis functions, (1a) can be conformed to the equivalent matrix form as,

$$[Z]_{N\times N}[I]_{N\times 1} = [Z_{pe} + Z_l]_{N\times N}[I]_{N\times 1} = [V]_{N\times 1} \tag{2a}$$

$$[Z_{pe}] = [R_{pe}] + j[X_{pe}],\ [Z_l] = [R_l] + j[X_l] \tag{2b}$$

The complex symmetric matrix $[Z_{pe}]$ arises due to the electric field integral equation (EFIE) operator in the lossless scenario [2] and the additional loss operator incorporates the loss matrix $[Z_l]$. The eigenmodes of the lossy objects can be computed using any of the following two decomposition methods [14],

$$[Z_{pe} + Z_l][U]_n = (1 + j\zeta_n)[R_{pe} + R_l][U]_n \tag{3a}$$

$$\text{or } ([Z_{pe} + Z_l][I]_n = (1 + j\lambda_n)[R_{pe}][I]_n \tag{3b}$$

It can be shown using the complex power balance relation of [3] that the characteristic modes U_n cannot diagonalize the far-field scattering matrix. The situation is quite similar to the formulation of lossy dielectric object in [3]. Hence, the far-field eigen patterns cannot be characterized using the formulation of (3a). So this paper considers the characteristic equation of (3b) for analysing the lossy structures. With further simplification of (3b),

$$[X_{pe} - jZ_l][I_n] = \lambda_n [R_{pe}][I_n] \tag{4}$$

The orthogonal properties of the eigenvectors $[I_n]$ can be defined as,

$$< [I_m]^*, [R_{pe}][I_n] > = \delta_{mn} \tag{5a}$$

$$< [I_m]^*, [X_{pe} - jZ_l][I_n] > = \lambda_n \delta_{mn} \tag{5b}$$

$$\text{where } \delta_{mn} = 0 \text{ if } m \neq n, \text{ else } 0 \tag{5c}$$

The weighting coefficients' column vector $[I]$ of (2a) can be expressed as a weighted sum of the column vectors $[I_n]$ of (4) as,

$$[I] = \sum_{i=1}^{N} \alpha_n [I_n] \tag{6}$$

Following (5a)-(5c),

$$\alpha_n = \frac{< [I_n]^*, [V] >}{1 + j\lambda_n} = \frac{< [I_n]^*, [V] >}{1 - Im.(\lambda_n) + j\ Re.(\lambda_n)} \tag{7}$$

The complex conjugation operation $'*'$ has been incorporated in the complex inner products of (5a), (5b), and (7) considering the probable complex nature of the eigenmode $[I_n]$. The real and imaginary parts of the complex eigenvalue λ_n are denoted by $Re.(\lambda_n)$ and $Im.(\lambda_n)$ respectively. For the n^{th} mode, the complex modal power consists of three components, the radiative power $(P_{R,n})$, the lost power $(P_{L,n})$ and the reactively stored power $(P_{X,n})$ which can be written using the orthogonality properties of (5a)-(5c) as,

$$\begin{aligned} P_{R,n} = |\alpha_n|^2,\ P_{L,n} = -Im.(\lambda_n)\ |\alpha_n|^2, \\ \text{and } P_{X,n} = Re.(\lambda_n)\ |\alpha_n|^2 \end{aligned} \tag{8}$$

For the lossless case, the $Im.(\lambda_n) = 0$ and $Im.([I_n]) = 0$. In the next stage, the following fundamental issues have been addressed,

1) How to determine the modes that will dominantly contribute to the resultant radiated emission from a given structure?
2) How to identify the characteristic modes that contribute significantly towards the resultant scattered field used in EMI/EMC characterisation?

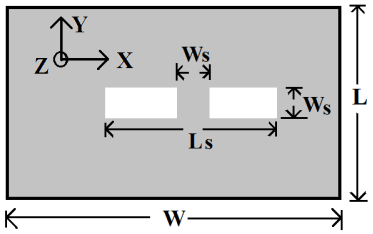

Fig. 1: Rectangular slotted plate with $W = \lambda/2$, $L = \lambda/2$, $L_s = \lambda/6$ and $W_s = \lambda/100$ at $f = 0.5$ GHz.

III. Modal Significance Measures

A. Radiation Cases

Effective excitation of a characteristic mode from a radiating structure depends on both the radiative and reactive modal power parameters of (8). For external resonance, the reactive modal power $P_{X,n}$ becomes minimum. Similarly for the maximum radiation at the resonating frequency, the radiated modal power $P_{R,n}$ needs to be maximum. Following (8) the ratio of the reactive and radiative power of the n^{th} mode can be written as,

$$\frac{P_{X,n}}{P_{R,n}} = Re.(\lambda_n) \tag{9}$$

For a very low value of $Re.(\lambda_n)$, there is possibility of the variables $P_{R,n}$ and α_n being simultaneously high. In line with

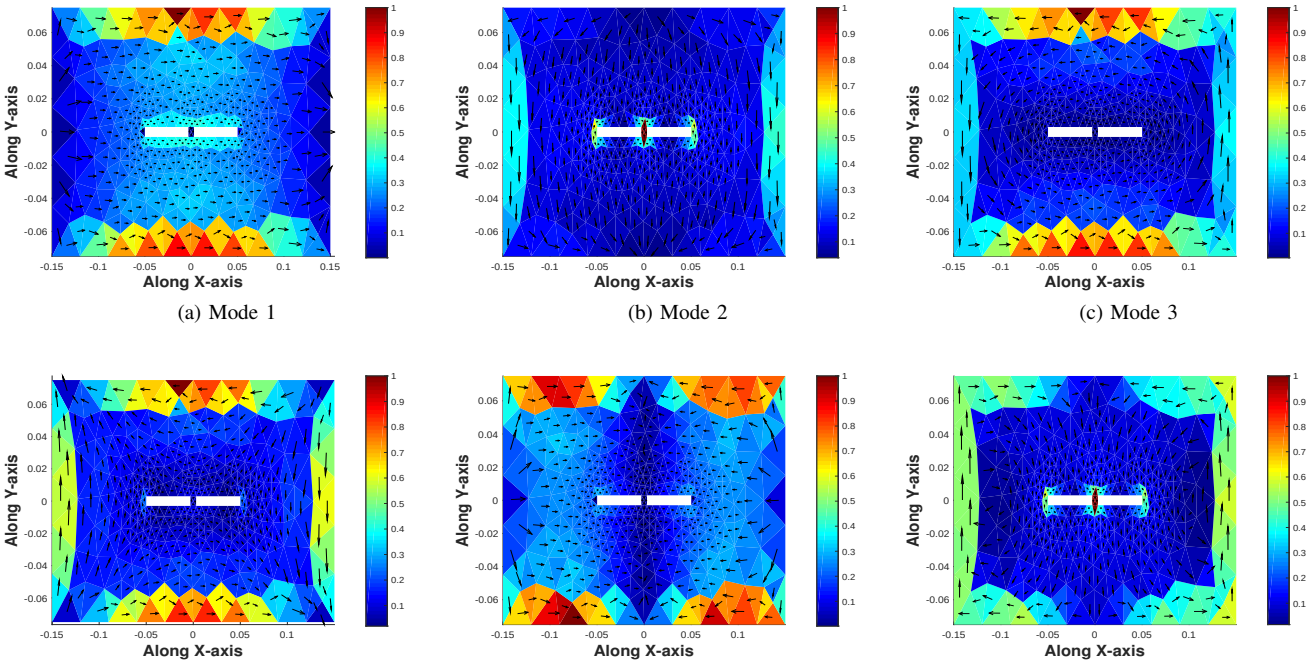

(a) Mode 1 (b) Mode 2 (c) Mode 3

(d) Mode 4 (e) Mode 5 (f) Mode 6

Fig. 2: First six eigencurrent modes ($\alpha_n \vec{J}_n$) of the plate of Fig.1 at $f = 0.5$ GHz. Modes are sorted as per Λ_n.

this logic, two different modal significance measures Δ_n and Λ_n were defined using only the eigenvalue in [5] and [6],

$$\Lambda_n = \frac{1}{\sqrt{[1 + [Re.(\lambda_n)]^2]}} \tag{10a}$$

$$\text{and} \quad \Delta_n = \frac{1}{\sqrt{1 + Re.(\lambda_n)}} \tag{10b}$$

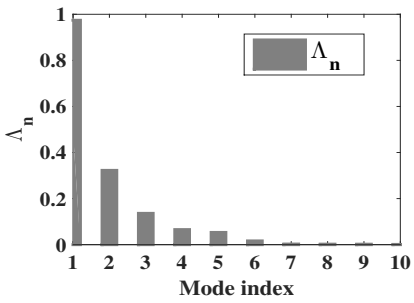

Fig. 3: Λ_n of the slotted rectangular plate of Fig.1 at $f = 0.5$ GHz.

To verify the suitability of the measures of (10a) and (10b), a slot-antenna type geometry with finite conductivity has been considered in Fig.1. The free-space wavelength at $f = 0.5$ GHz is denoted by λ. The loss matrix Z_l of the plate of Fig.1 has been calculated following the formulation of (1a)–(1f) using [17] – [19] in MATLAB [20]. In this example, the thickness (t) and conductivity (σ) of the plate has been considered to be 18 μm and 10^6 S/m. The total number of triangles was 494 in the surface patch formulation of the structure. Feed location has been chosen at the centre of the plate.

The characteristic modes have been computed in MATLAB following (4). Sorting the modes in the ascending order of Λ_n, the first six eigencurrent modes $\alpha_n \vec{J}_n$ are shown in Fig.2a–2f. For comparison, each mode has been normalised with respect to its maximum amplitude (i.e., $\alpha_n \vec{J}_n / max(|\alpha_n \vec{J}_n|)$). The n^{th} characteristic mode $\vec{J}_n$ is related to the n^{th} eigenvector $[I_n]$ as,

$$\vec{J}_n = \sum_{i=1}^{N} I_n(i) \vec{f}_i(r_i), \; r_i \in S \tag{11}$$

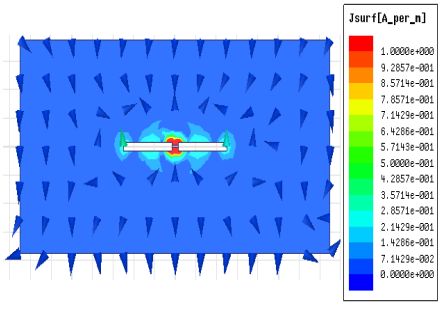

Fig. 4: HFSS-based current distribution of the slotted rectangular plate of Fig.1 at $f = 0.5$ GHz.

The i^{th} basis function and the surface area of the radiating structure are denoted by $\vec{f}_i$ and S respectively. Number of basis functions used to discretize the structure is assumed to be N in (11). Values of Λ_n corresponding to the six modes of Fig.2a–2f are shown in Fig.3. Apparent observation of Fig.3 indicates that only Mode 1 of Fig.2a is the most dominant mode for the slotted structure of Fig.1. For verification, the

slot-antenna has been simulated in a differential technique based full-wave simulator HFSS [21] and the resultant current distribution is shown in Fig.4. For the HFSS simulation, a lumped-port delta-gap excitation with the gap width of $\lambda/200$ has been considered. It is interesting to note that Fig.4 has maximum similarity to Mode 2 and Mode 6 of Fig.2b and 2f, instead of Mode 1 of Fig.2a. Thus, the eigenvalue-based modal measure of (10a) seems to be inaccurate enough to predict the effective dominant mode of a radiating structure.

TABLE I: Eigenvalues of the plate of Fig.1 at $f = 0.5$ GHz

Mode index	$Re.(\lambda_n)$	Nature
Mode 1	0.23	inductive
Mode 2	-2.93	capacitive
Mode 3	7.28	inductive
Mode 4	-15.24	capacitive
Mode 5	-18.75	capacitive
Mode 6	61.03	inductive

For the other eigenvalue-based measure Δ_n of (10b), the eigenvalues of the first 6 modes of Fig.2a–2f are given in Table I. It is obvious from Table I that the measure of (10b) will be imaginary for Mode 2, Mode4 and Mode 5. In general, the measure Δ_n will be imaginary for $Re.(\lambda_n) < -1$. Thus, the measure of (10b) is also not suitable enough in characterizing the modal significance of a radiating element.

One major limitation of the eigenvalue-based measures is that both Λ_n and Δ_n solely depend on $Re.(\lambda_n)$. However, being a ratio of the radiated and reactive power, $Re.(\lambda_n)$ is insufficient to provide individual characterization of $P_{R,n}$ and $P_{X,n}$. Thus, the smaller value of $Re.(\lambda_n)$ or higher value of Λ_n cannot ensure that the corresponding mode possesses sufficient modal wightage to be effectively excited. To overcome the limitation of Λ_n, another metric was proposed in [6] where the dominant modes for maximum radiation was suggested to choose using a relative measure of the radiated power $P_{R,n}$. Now let the object be discretized with N number of RWG basis functions [18]. Then the radiative power of the n^{th} mode can be written with delta-gap approximation as,

$$P_{R,n} = \frac{|[I_n(r_f)]l_e|^2}{[1 - Im.(\lambda_n)]^2 + [Re.(\lambda_n)]^2} \tag{12}$$

The length of the edge of the basis closest to the feed-location (r_f) is denoted by l_e in (12).

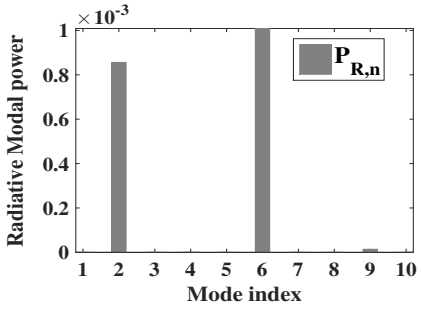

Fig. 5: $P_{R,n}$ of the slotted plate of Fig.1 at $f = 0.5$ GHz.

Variation of the radiative modal power is shown in Fig.5. The ordering of the $P_{R,n}$ does not actually follow the sequence of (10a) in Fig.5. Mode 1 of Fig.2a has lower radiated power compared to Mode 2 and Mode 6 in Fig.5. If the radiative measure of (12) is followed, Mode 6 seems to be the most dominant mode in Fig.5. However, the similarity of Fig.2b is relatively higher to total current distribution of Fig.4, in comparison to Mode 6.

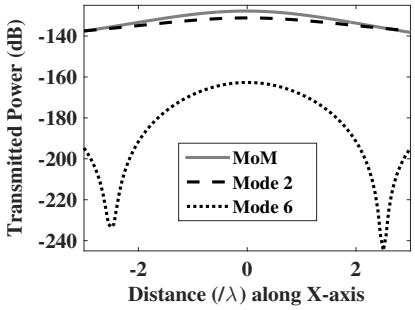

Fig. 6: Transmitted power along the X-directed observation line at $f = 0.5$ GHz.

For further quantitative investigation, let us consider a field observation line parallel to the slotted structure of Fig.1, i.e., along the X-axis. The transmitted power contributed by of Mode 2 and Mode 6 have been compared to the power computed using conventional MoM technique along the observation line in Fig.6. The closeness with the MoM-based total power is higher for Mode 2 compared to Mode 6 in Fig.6. So, the question is whether the study of only the radiative component can provide correct prediction of the dominant modes in radiated emission analysis. The literature of [22] can shed some light regarding this issue.

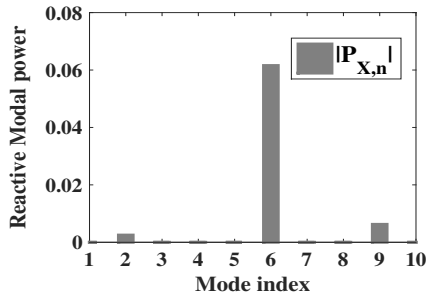

Fig. 7: $P_{X,n}$ of the slotted plate of Fig.1 at $f = 0.5$ GHz.

Following [22], the energy flow velocity seems to be one important factor for efficient radiation. It physically indicates how the energy moves in a certain location in space for a given radiating structure's field distribution which is linearly related to the induced current density vector. It has been found in [22] that the non-zero reactive power slows down the velocity of instantaneous power flow. As a consequence, the modes having higher amount of $P_{X,n}$ cannot contribute significantly the power received at distant location. So the selection of dominant characteristic modes should also consider on the corresponding reactive modal power $P_{X,n}$. Similar to $P_{R,n}$ of (12), the reactive modal power of the n^{th} mode can be

written as,

$$P_{X,n} = \frac{Re.(\lambda_n)\ |[I_n(r_f)]l_e|^2}{[1 - Im.(\lambda_n)]^2 + [Re.(\lambda_n)]^2} \tag{13}$$

As shown in Fig.7, the reactive modal power of Mode 6 is quite high compared to Mode 2. The higher value of $P_{X,6}$ leads to its less contribution in the transmitted power of Fig.6. It can be seen from Fig.5 and 7 that $P_{X,6}$ is significantly higher with respect to its radiative component $P_{R,6}$. It can explain the higher similarity of Mode 2 to the HFSS-based result of Fig.4. Thus, the characterisation of only the radiated power $P_{R,n}$ of (12) cannot assure proper selection of dominant modes. With an objective to overcome the limitations of the previously reported modal measures, this paper introduces a constrained optimization approach for identifying the group of modes dominantly responsible for the radiated emission from a given structure. The search of dominant modes at a particular frequency can be defined as,

$$\begin{aligned} &\underset{n\in[1,N]}{\text{maximize}} \quad \frac{|[I_n(r_f)]l_e|^2}{[1 - Im.(\lambda_n)]^2 + [Re.(\lambda_n)]^2} \\ &\text{subject to} \quad \frac{1}{\sqrt{[1 + [Re.(\lambda_n)]^2]}} \geq \Lambda_{threshold} \end{aligned} \tag{14}$$

TABLE II: Comparison of modal ranking of the plate of Fig.1 at $f = 0.5$ GHz

Modal measure	Modal rank = 1	Modal rank = 2
Λ_n	Mode 1	Mode 2
$P_{R,n}$	Mode 6	Mode 2
(14)	Mode 2	Mode 6

Main advantage of (14) is that it considers both components of the complex modal power. The threshold parameter $\Lambda_{threshold}$ sets the level of the reactively stored modal power compared to the corresponding modal radiative power. In the next stage, the modes with higher or equivalent value of $\Lambda_{threshold}$ are sorted as per the radiative modal measures of (12). For illustration, the same finitely conducting slot-antenna example of Fig.1 has been considered. Sorting the modes as per (14), the modal ranking has been compared with the previous measures in Table II. The constrained method of (14) indicates Mode 2 as the most significant mode of the considered structure of Fig.1. The results of Fig.4 and 6 also justify the suitability of (14). Thus, the proposed *modal metric* of (14) can be utilized as an efficient tool to estimate the radiated emission [7] and [8]. The succeeding discussion extends the modal significance measure for the scattering scenarios which may find practical applications like in electromagnetic shielding analysis.

B. Scattering Cases

Unlike the transmitting antenna design problems, the incident field is not concentrated in a particular location in the scattering problem. Rather it covers a distributed region over the object's surface. Hence, the numerator of α_n in (7) can no longer be approximated as $||[I_n(r_f)]|l_e|^2$. So the measures of (12) and (14) will not reflect the distributive nature of the scattering phenomena. Since no information of the excitation signal is available in the conventional measure of (10a), it is also not capable of correctly characterizing the modal dominance. The succeeding example further clarifies this limitation. As discussed previously, the net outward flow of power depends on choosing the characteristic mode that will be excited effectively. The excitation of a particular mode is controlled by both $P_{R,n}$ and $P_{X,n}$. Both $P_{R,n}$ and $P_{X,n}$ are linearly proportional to $|\alpha_n|^2$ [2] where,

$$\begin{aligned} |\alpha_n| = |\frac{< [I_n]^*, [V] >}{1 + j\lambda_n}| &= |\frac{< [I_n]^*, [V] >}{1 - Im.(\lambda_n) + j\ Re.(\lambda_n)}| \\ &= \frac{| < [I_n]^*, [V] > |}{\sqrt{[1 - Im.(\lambda_n)]^2 + [Re.(\lambda_n)]^2}} \end{aligned} \tag{15}$$

So it is required to choose the significant modes based on the absolute magnitude of α_n, provided its reactive power lies in the lower level. Considering the distributive nature of the incident field, the dominant eigenmodes can be determined following the two-level sorting procedure as,

$$\begin{aligned} &\underset{n\in[1,N]}{\text{maximize}} \quad \frac{| < [I_n]^*, [V] > |}{\sqrt{[1 - Im.(\lambda_n)]^2 + [Re.(\lambda_n)]^2}} \\ &\text{subject to} \quad \frac{1}{\sqrt{[1 + [Re.(\lambda_n)]^2]}} \geq \Lambda_{threshold} \end{aligned} \tag{16}$$

The measure of (16) is mathematically complete in the sense that it contains all the influencing parameters that control the characteristic information of a scattering structure, i.e., the incident signal, the eigenvector and the eigenvalue. The polarization mismatch between the incident vector $[V]$ and the corresponding characteristic mode $[I_n]$ is reflected by the numerator of (16). As exemplified later, phase difference between the incident wave and the corresponding mode can play crucial role in the resultant scattered field which is commonly used in computing the shielding effectiveness of a given structure. It can be noted from (8) that low value of $Re.(\lambda_n)$ assures the reactive modal power $P_{X,n} = Re.(\lambda_n)|\alpha_n|^2$ is low to attain resonance. The next level sorting using $|\alpha_n|$ further determines the strongly resonant mode having sufficient radiative power to be excited.

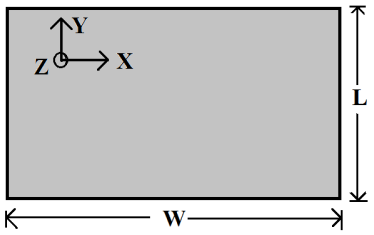

Fig. 8: Schematic of the lossy rectangular plate. $W = 0.5\lambda$ and $L = 0.3\lambda$ at $f = 1$ GHz.

To compare the proposed scattering measure of (16) to the conventional modal significance measure of (10a), let us consider the rectangular plate of Fig.8. The thickness (t) and conductivity (σ) of Fig.8 has been set as 18 μm and 10^6 S/m. A total 200 triangles have been considered in the meshing of the structure.

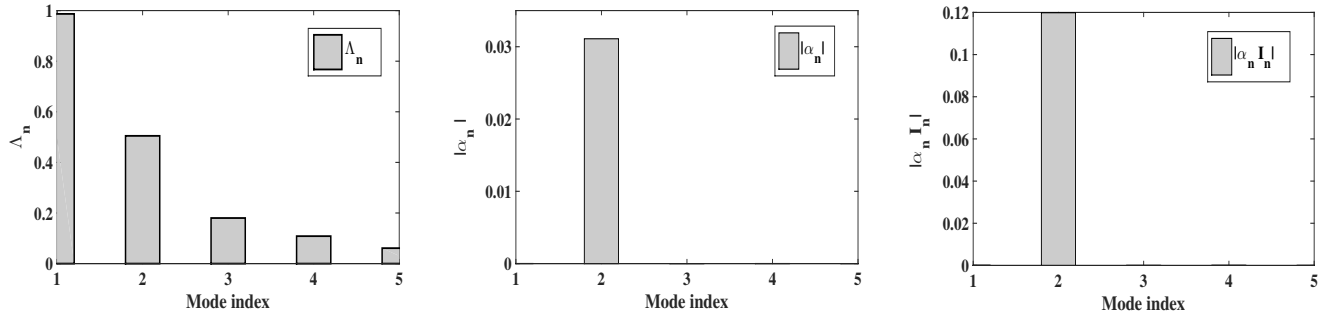

(a) $|\Lambda_n|$ (b) $|\alpha_n|$, Y-pol. incidence (c) $|\alpha_n I_n|$, Y-pol. incidence

Fig. 9: Comparison of various modal parameters: (a) Λ_n, (b) $|\alpha_n|$ and (c) $|\alpha_n I_n|$ variation with unit amplitude Y-polarized plane-wave incidence.

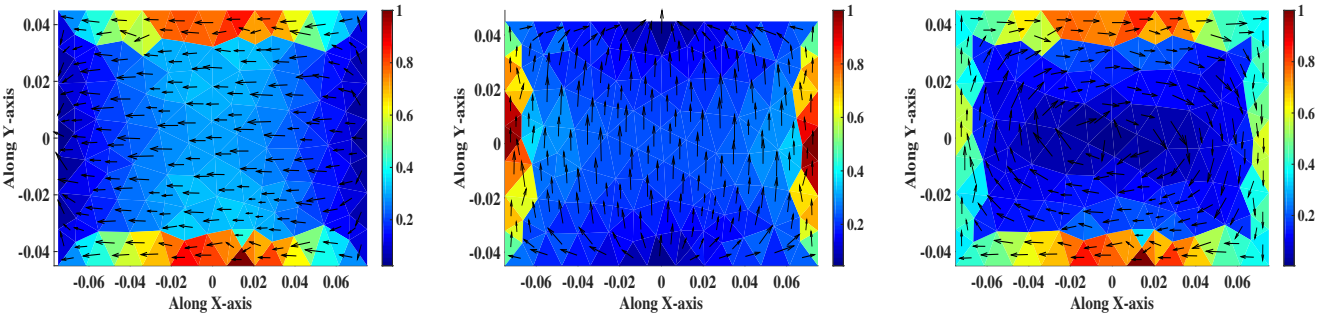

(a) $\vec{J}_{1,TCM}$, Y-pol. incidence (b) $\vec{J}_{2,TCM}$, Y-pol. incidence (c) $\vec{J}_{3,TCM}$, Y-pol. incidence

Fig. 10: Various modal current distribution due to unit amplitude Y-polarized plane-wave incidence.

Sorting the eigen modes as per (10a), the variation of (10a), (16) and the modal current norm $|\alpha_n I_n|$ has been shown in Fig.9a–9c. Following the conventional measure of Λ_n, only the 1^{st} mode seems to be apparently significant in Fig.9a. However, it can be noted from Fig.9b and 9c that the 2^{nd} mode appears to be effectively significant when Y-polarized unit amplitude plane wave incidence is considered. To further understand the reason behind such phenomena, it is important to concentrate on the current distribution of the first three modes in Fig.10a–10c.

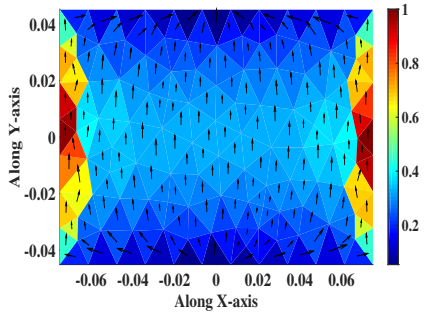

Fig. 11: MoM-based current distribution due to unit amplitude Y-polarized plane-wave incidence.

The 1^{st} mode seems to be X-polarized in Fig.10a whereas the 2^{nd} one is Y-polarized in Fig.10b. The 3^{rd} mode is circular in nature in Fig.10c. It can be noted from (16) that the numerator of α_n controls the polarization angle between the incident field and the corresponding mode. Since the 2^{nd} mode is Y-polarized, the polarization mismatch will be minimum for the Y-polarized plane-wave incidence. This leads to the fact of being higher value of $|\alpha_n|$ and $|\alpha_n I_n|$ for the 2^{nd} mode in Fig.9b and 9c. For further validation, the MoM-based current distribution has been shown in Fig.11 which seems to have maximum similarity with the 2^{nd} mode of Fig.9b. Thus, for this particular scenario, the 2^{nd} mode is mostly dominant. So in a generic sense, the measure of (16) can play better role in representing the modal dominance compared to the conventional modal significance measure of (10a) for scattering analysis.

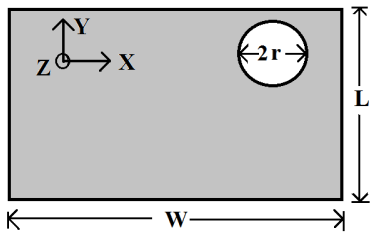

Fig. 12: Schematic of the circularly slotted rectangular plate, $W = 0.5\lambda, L = 0.3\lambda$ and $r = \lambda/50$ at $f = 1$ GHz.

The succeeding section employs the modal approach for the shielding analysis.

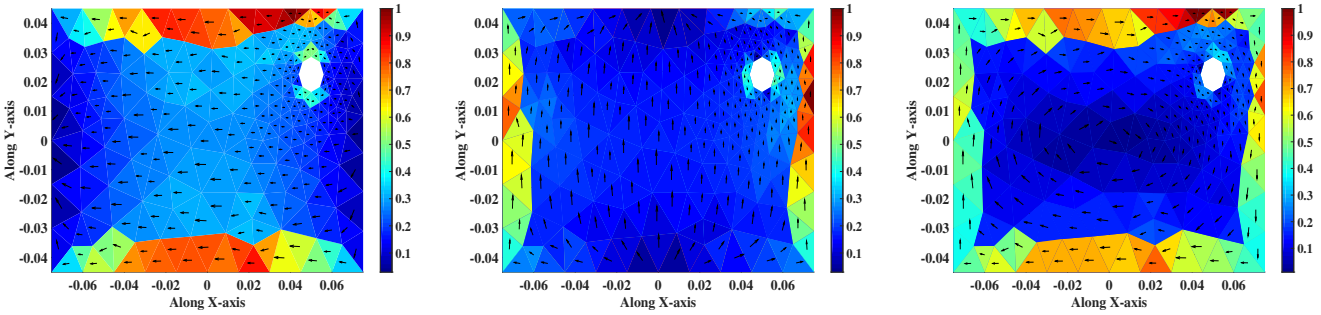

(a) Mode 1 (b) Mode 2 (c) Mode 3

Fig. 13: Normalised distribution of the first 5 dominant characteristic current modes: (a) $\vec{J}_1$, (b) $\vec{J}_2$, (c) $\vec{J}_3$.

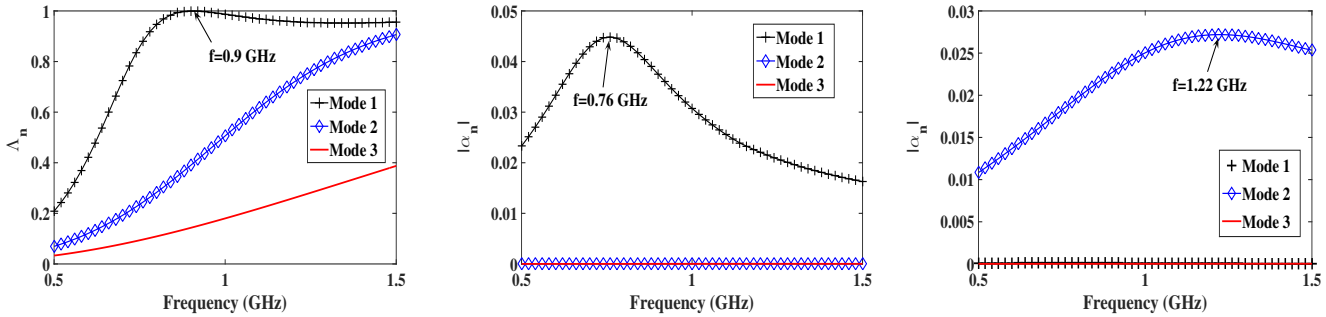

(a) Λ_n (b) Mode 2 (c) Mode 3

Fig. 14: Frequency variation of (a) λ_n; (b) $|\alpha_n|$ for X-pol. plane wave incidence and (c) $|\alpha_n|$ for Y-pol. plane wave incidence.

IV. Application:-Shielding Effectiveness Prediction

Contrary to the antenna design examples, EMC and signal integrity is interested in reducing the radiated power from different printed circuit elements using the characteristic modes in [7] and [8] where the dominant modes have been determined using the eigenvalue-based modal measure. As stated in the previous discussion, the measure of (16) will be more accurate compared to the eigenvalue-based measure of (10a) for analysing the RF exposure in the neighbouring objects. The RF exposure of some arbitrary shaped apertures have been previously analysed using computational electromagnetic techniques in [12] and [13] which requires the computation of the scattered field from the object of interest.

In this regard, the present manuscript utilizes the characteristic modes to relatively gauge the shielding behaviour. The shielding towards the RF signal is generally characterized by the parameter shielding effectiveness (SE) [13],

$$SE(dB) = 20log\frac{|\vec{E}_i|}{|\vec{E}_t|} \tag{17}$$

The field incident on the object is denoted by $\vec{E}_i$. $\vec{E}_t$ indicates the field emerging from the object. Implying the TCM, the outgoing field $\vec{E}_t$ can be expressed as the weighted sum of N number of characteristic field patterns $\vec{E}_n$,

$$\vec{E}_t = \sum_{i=1}^{N} \alpha_n \vec{E}_n \tag{18}$$

If the incident signal amplitude is assumed as unity, the SE parameter can be written as,

$$SE(dB) = -20log|\vec{E}_t| = -20log|\sum_{i=1}^{N} \alpha_n \vec{E}_n| \tag{19}$$

Since the characteristic pattern $\vec{E}_n$ is linearly related to the characteristic current mode $\vec{J}_n$, the SE parameter can be relatively gauged by the parameter $\alpha_n\vec{J}_n$. At a particular frequency, the resultant current density vector $\vec{J}$ or the outward field $\vec{E}_t$ is expressed as the sum of the first few, say U number of dominant modes. So the following parameter $SE_{J,TCM}$ can give a hint of the shielding nature of the considered object towards the RF exposure,

$$SE_{J,TCM}(dB) = 20log|\sum_{i=1}^{U} \alpha_n \vec{J}_n| \tag{20}$$

The selection of the dominant characteristic modes can be computed using the proposed measure of (16). For the sake of comparing the convergence performance, let us consider an equivalent MoM parameter $SE_{J,MoM}$,

$$SE_{J,MoM}(dB) = 20log|\vec{J}_{MoM}| \tag{21}$$

$\vec{J}_{MoM}$ represents the induced current density vector using the conventional MoM technique [1].

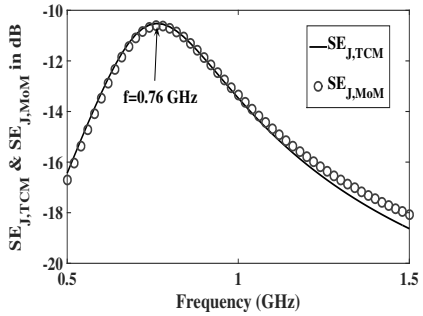

Fig. 15: $SE_{J,TCM}$ and $SE_{J,MoM}$ vs frequency with $U = 3$ for X-pol. plane wave incidence.

For validation purposes, the slotted PEC plate of Fig.12 has been taken as a template. The centre of the slot is assumed to be at $(L/3, W/4, 0)$. The number of triangles is 298 for the discretization of the plate's surface. The first three modes have been shown in Fig.13a-13c where the first two modes are found to be respectively X- and Y-polarized. The modes have been sorted following (10a). If the frequency variation of (10a) is followed in Fig.14a, the 1^{st} mode of Fig.13a seems to be the only significant mode of the structure. In the next stage, two different types of wave incidence have been considered and the corresponding variation of $|\alpha_n|$ are shown in Fig.14b and 14c. When X-polarized plane wave incidence is considered, the X-polarized 1^{st} mode of Fig.13a becomes the dominant one in Fig.14b. Similarly, when Y-polarized plane-wave falls upon the structure, the Y-polarized 2^{nd} mode of Fig.13b becomes mostly dominant in Fig.14c.

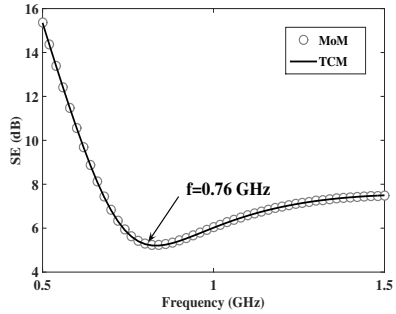

Fig. 16: SE vs frequency with $U = 3$ for the X-pol. plane wave incidence.

Following (10a) and Fig.14a it apparently seems that the maximum RF interaction occurs at $f = 0.9$ GHz. However, it can be noted from the comparison of Fig.14a and 14b that the RF exposure will be effectively maximum at $f = 0.76$ GHz for the X-polarized incidence. Similarly, it is at $f = 1.22$ GHz for the Y-polarized incidence Fig.14c. To verify in more details, the current-based shielding parameters $SE_{J,TCM}$ and $SE_{J,MoM}$ have been compared in Fig.15 where the convergence performance is also close. The field based shielding parameter of (19) has been shown in Fig.10. In both cases of Fig.15 and 10, the frequency of maximum RF exposure seems to be the one reflected by the frequency variation of $|\alpha_n|$ in Fig.14b. So the measure of (14) will be suitable not only for determining the dominant modes in scattering, but also for correct prediction of the RF exposure. Another beneficial contribution of the characteristic mode theory is the parameter of (19). It can be recalled at this point that the computation of SE using the conventional formulation of (17) is necessarily a two-step process. The first step calculates the induced current density vector and in the succeeding step, the outward field has to be computed. One main advantage of (19) is that it conforms the SE prediction into a single step process with detailed insight of each individual mode. Once the dominant modes are identified, the slot can be adjusted accordingly to experience minimum signal interference effects.

So, the major contribution of the present work can be summed up a systematic guideline to choose a suitable modal metric using the underlying physical insight. Two separate measures have been proposed in (14) and (16) for determining the dominant characteristic modes in radiating and scattering problems respectively. Later, a modal parameter has been defined in (20) for approximating the shielding response. Considering the gradual demand of miniaturised design with multiple components, the proposed measures can be improvised in various EMI/EMC applications like the determination of the radiation hotspot(/s) [8], for reduction of the radiated emission from the PCB components [9] and [23], and for the relative prediction of the RF exposure [12].

V. Conclusions

Following the application of the Eigen mode theory, this paper explores the selection mechanism of dominant characteristic modes of a given structure. Separate modal measures have been gradually formulated for characterizing the radiation and scattering phenomena. Later a simple alternate technique has been discussed for the shielding prediction using the modal information of the structure under consideration. The crux of the proposed work lies in the fact that the modal measure should be chosen based on the underlying physical mechanism of the related application.

References

[1] R. F. Harrington, *Field computation by moment methods*. Wiley-IEEE Press, 1993.

[2] R. Harrington and J. Mautz, "Theory of characteristic modes for conducting bodies," *IEEE Trans. Antennas Propagat.*, vol. 19, no. 5, pp. 622–628, 1971.

[3] R. Harrington, J. Mautz, and Y. Chang, "Characteristic modes for dielectric and magnetic bodies," *IEEE Trans. Antennas Propagat.*, vol. 20, no. 2, pp. 194–198, 1972.

[4] R. Garbacz and R. Turpin, "A generalized expansion for radiated and scattered fields," *IEEE Trans. Antennas Propagat.*, vol. 19, no. 3, pp. 348–358, 1971.

[5] M. Cabedo-Fabres, E. Antonino-Daviu, A. Valero-Nogueira, and M. F. Bataller, "The theory of characteristic modes revisited: A contribution to the design of antennas for modern applications," *IEEE Antennas Propag. Mag.*, vol. 49, no. 5, pp. 52–68, 2007.

[6] J. Ethier and D. McNamara, "Modal significance measure in characteristic mode analysis of radiating structures," *Electron. Lett.*, vol. 46, no. 2, pp. 107–108, 2010.

[7] Q. Wu, H.-D. Bruns, and C. Schuster, "Characteristic mode analysis of radiating structures in digital systems," *IEEE Electromagn. Compat. Mag.*, vol. 5, no. 4, pp. 56–63, 2015.

[8] Y. S. Cao, Y. Wang, L. Jiang, A. E. Ruehli, J. Fan, and J. L. Drewniak, "Quantifying EMI: a methodology for determining and quantifying radiation for practical design guidelines," *IEEE Trans Electromagn Compat*, vol. 59, no. 5, pp. 1424–1432, 2017.
[9] S. Ghosal, A. De, A. Chakrabarty, and R. M. Shubair, "Analysis of slot loading in elliptical patch- a characteristic mode approach," *IEEE ANTEM 2018, Canada*, 2018.
[10] M. Rothenhäusler and F. Gronwald, "Characteristic mode analysis of HIRF-and DCI-excitations of an aircraft structure," in *Electromagnetic Compatibility-EMC EUROPE, 2017 International Symposium on*. IEEE, 2017, pp. 1–6.
[11] S. H. Yeung and C.-F. Wang, "Exploration of characteristic mode theory for electromagnetic compatibility modeling," in *2018 IEEE International Symposium on Electromagnetic Compatibility and 2018 IEEE Asia-Pacific Symposium on Electromagnetic Compatibility (EMC/APEMC)*. IEEE, 2018, pp. 1278–1282.
[12] D. G. Lopez, M. Ignatenko, and D. S. Filipovic, "Eigenmode prediction of high RF exposure frequency region inside vehicles," *IEEE Trans Electromagn Compat*, vol. 59, no. 1, pp. 43–47, 2017.
[13] J. Chen, J. Guo, and C. Tian, "Analyzing the shielding effectiveness of a graphene-coated shielding sheet by using the HIE-FDTD method," *IEEE Trans Electromagn Compat*, vol. 60, pp. 362–367, 2018.
[14] R. Li, D. McNamara, and G. Wei, "Characteristic modes evaluation for metallic small antennas with unidirectional pattern," *IEEE Antennas Wireless Propagat. Lett.*, vol. 16, pp. 3026–3029, 2017.
[15] M. Shahpari and D. V. Thiel, "The impact of reduced conductivity on the performance of wire antennas," *IEEE Trans. Antennas Propagat.*, vol. 63, no. 11, pp. 4686–4692, 2015.
[16] T. K. Sarkar, E. L. Mokole, and M. Salazar-Palma, "An expose on internal resonance, external resonance, and characteristic modes," *IEEE Trans. Antennas Propagat.*, vol. 64, no. 11, pp. 4695–4702, 2016.
[17] R. Maaskant, D. J. Bekers, M. J. Arts, W. A. van Cappellen, and M. V. Ivashina, "Evaluation of the radiation efficiency and the noise temperature of low-loss antennas," *IEEE Antennas Wireless Propagat. Lett.*, vol. 8, pp. 1166–1170, 2009.
[18] S. Rao, D. Wilton, and A. Glisson, "Electromagnetic scattering by surfaces of arbitrary shape," *IEEE Trans. Antennas Propagat.*, vol. 30, no. 3, pp. 409–418, 1982.
[19] S. N. Makarov, *Antenna and EM Modeling with MATLAB*. Wiley-Interscience,, 2002.
[20] MATLAB, *version 7.10.0 (R2010a)*. Natick, Massachusetts: The MathWorks Inc., 2010.
[21] HFSS, *ver. 2015*. Canonsburg, Pennsylvania, USA: Ansys Inc., 2015.
[22] C. A. Valagiannopoulos and A. Alu, "The role of reactive energy in the radiation by a dipole antenna," *IEEE Trans. Antennas Propagat.*, vol. 63, no. 8, pp. 3736–3741, 2015.
[23] S. Piersanti and A. Orlandi, "Genetic algorithm optimization for the total radiated power of a meandered line by using an artificial neural network," *IEEE Trans Electromagn Compat*, vol. 60, no. 4, pp. 1014–1017, 2018.

Sandip Ghosal (S'15) received the B.Tech. degree in Electronics and Communication Engineering from Kalyani Government Engineering College, Kalyani, India, in 2012, and M.E. degree in Microwave Communication from Indian Institute of Engineering, Science and Technology Shibpur, Shibpur, India, in 2014. He is presently working towards the Ph.D. degree at the Department of Electronics and Electrical Communication Engineering in Indian Institute of Technology Kharagpur, Kharagpur, India.

His current research interests include computational techniques for electromagnetic applications.

Arijit De (S'04–M'11) received the B.Tech. degree from IIT Kharagpur, Kharagpur, India, in 2004, and the Ph.D. degree from Syracuse University, Syracuse, NY, USA, in 2010.

He joined the Department of Electronics and Electrical Communication Engineering, IIT Kharagpur, as an Assistant Professor in 2010, where he has been as an Associate Professor, since 2016. He has co-authored the book titled "Time and Frequency Domain Solutions of EM problems using Integral Equation and a Hybrid Methodology" published by Wiley and IEEE Press in 2010. His current research interests include computational electromagnetics and radar signal processing.

Dr. De received the Young Scientist Award from URSI in 2011.

Alistair P. Duffy (M'93–SM'04–F'15) received the B.Eng. (Hons.) degree in electrical and electronic engineering and the M. Eng. degree from the University College, Cardiff, U.K., in 1988 and 1989, respectively. He received the Ph.D. degree from Nottingham University, Nottingham, U.K., in 1993 for his work on experimental validation of numerical modeling and the MBA from the Open University in 2003.

He is currently a Professor in electromagnetics at De Montfort University, Leicester, U.K, the Director of the Institute of Engineering Sciences and a Guest Professor at Harbin Institute of Technology, Harbin, China. He is the author of over 200 articles published in journals and presented at international symposia. His research interests include CEM validation, communications cabling, and technology management.

Alistair is a Fellow of the IEEE and of the Institution of Engineering and Technology (IET). He is Vice President for Conferences in the IEEE EMC Society Board of Directors and Associate Editor of the IEEE Transactions on EMC as well as Chair of the IEEE EMC Society Standards Development and Education Committee. He is a member of the Board of Directors of the IWCS.

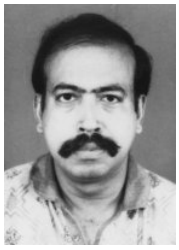

Ajay Chakrabarty (M'87–M'90) received the B.Tech (with Hons.) degree in electronics and electrical communication engineering, the M.Tech degree in microwave engineering, and the Ph.D. degree from the Department of Electronics and Electrical Communication Engineering, I.I.T, Kharagpur, India in 1975, 1977, and 1982, respectively. He joined the Electronics and Electrical Communication Engineering Department, I.I.T., Kharagpur, as a Lecturer in 1980. Since 1994, he has been serving as a Professor at the same department. He was a visiting faculty at Syracuse University, NY from 1990 to 1992. His present areas of interest include antenna theory, slot and waveguide radiator, phased array techniques, EMI/EMC, ESD, and numerical techniques.